Unusual Hyperfine Interaction of Dirac Electrons and NMR Spectroscopy in Graphene

Balázs Dóra[1] and Ferenc Simon[2]

[1]Max-Planck-Institut für Physik Komplexer Systeme, Nöthnitzer Straße 38, 01187 Dresden, Germany
[2]Budapest University of Technology and Economics, Institute of Physics and Solids in Magnetic Fields Research Group, Hungarian Academy of Sciences, P.O. Box 91, H-1521 Budapest, Hungary

(Received 24 March 2009; published 15 May 2009)

A theory of nuclear magnetic resonance (NMR) in graphene is presented. The canonical form of the electron-nucleus hyperfine interaction is strongly modified by the linear electronic dispersion. The NMR shift and spin-lattice relaxation time are calculated as a function of temperature, chemical potential, and magnetic field, and three distinct regimes are identified: Fermi-, Dirac-gas, and extreme quantum limit behaviors. A critical spectrometer assessment shows that NMR is within reach for fully ^{13}C enriched graphene of reasonable size.

DOI: 10.1103/PhysRevLett.102.197602 PACS numbers: 76.60.−k, 71.20.Tx, 85.75.−d

Nuclear magnetic resonance (NMR) is a powerful spectroscopic tool [1] and an architecture for quantum information processing [2,3]. Both of these applications are possible due to the weak interaction of the nucleus with its environment. This interaction is sufficient to probe the electronic state of its vicinity, which yields information about the local electron bonds or about the correlated behavior of electrons as, e.g., in superconductors [4]. NMR quantum computing exploits that nuclei are well isolated from the environment; thus, there is a longer time window for the manipulation of the nuclear state.

For both kinds of applications, the important NMR parameters are the shift of the NMR resonance with respect to a standard and the decay of the longitudinal magnetization to its equilibrium value, the spin-lattice relaxation time T_1. These were extensively studied in solid state systems both theoretically and experimentally [1,5]. However, the body of NMR experiments was focused on three-dimensional systems which stemmed from the unavailability of stable, inherently two-dimensional materials. The discovery of graphene, a single stable sheet of carbon atoms in a hexagonal lattice [6], enables studies of an exactly two-dimensional system. Its quasiparticles follow a linear band dispersion, causing the electrons to behave as massless Dirac fermions, which gives rise to unique transport and magnetic properties [7].

In a metal, the NMR measurables are most affected by the surrounding electrons through the electron-nuclear hyperfine interaction (HFI). The standard, textbook form of the HFI of nuclei and conduction electrons leads to the Hamiltonian $H_{\rm HFI} = H_{\rm orb} + H_{\rm spin}$ [5]:

$$H_{\rm orb} = \frac{\mu_0}{4\pi} g \mu_B^* \gamma_n \mathbf{I} \frac{\mathbf{r}\times\mathbf{p}}{r^3},$$
$$H_{\rm spin} = \frac{\mu_0}{4\pi} g \mu_B \hbar \gamma_n \mathbf{I}\left(\frac{\mathbf{S}r^2 - 3\mathbf{r}(\mathbf{S}\mathbf{r})}{r^5} - \frac{8\pi}{3}\mathbf{S}\delta(\mathbf{r})\right). \quad (1)$$

$H_{\rm orb}$ is due to the electron orbital magnetism, and $H_{\rm spin}$ contains the electron spin-dipole and the Fermi-contact interactions. μ_0 is the permeability of free space, γ_n is the nuclear gyromagnetic ratio, $\mathbf{I}$ is the nuclear spin, and $g \approx 2$ is the g factor of the electrons. $\mathbf{S}$, $\mathbf{p}$, and $\mathbf{r}$ are the electron spin, momentum, and vector operators, respectively. μ_B is the Bohr magneton, and $\mu_B^* = \mu_B m/m^*$ is the effective orbital Bohr magneton [8], where m^* is the effective mass and m is the mass of a free electron.

It is not obvious how to generalize the orbital term of the HFI to massless Dirac fermions. Second, the unique properties of the conduction electrons of graphene are expected to give rise to a unique NMR behavior. For example, deviation from the Korringa relation [1], that is an important benchmark of non-Fermi liquids, is expected.

Here we show that the canonical description of the hyperfine interaction is modified for the massless Dirac fermions, and we derive the corresponding hyperfine Hamiltonian. We identify different regimes based on the NMR measurables: Fermi-, Dirac-gas, and extreme quantum limit behaviors. We discuss the feasibility of NMR on graphene with a critical assessment of spectrometer performance.

The low energy excitations in graphene are described by the two-dimensional Dirac equation [7]:

$$H = v_F(\sigma_x p_x + \sigma_y p_y), \quad (2)$$

where $v_F \approx 10^6$ m/s is the Fermi velocity of graphene, and the pseudospin variables (Pauli matrices σ) spring from the two-sublattice structure. The HFI in graphene is derived following Abragam [5] by treating the nucleus as a magnetic dipole with $\mathbf{m} = \hbar\gamma_n\mathbf{I}$. Its vector potential $\mathbf{A}(\mathbf{r}) = \frac{\mu_0}{4\pi}\frac{\mathbf{m}\times\mathbf{r}}{r^3}$ is inserted into the kinetic momentum as $\mathbf{p} \to \mathbf{p} + e\mathbf{A}$ in addition to the electron and nuclear Zeeman terms. This calculation gives the effective HFI

$$H_{\rm HFI}^{\rm gr} = \frac{\mu_0}{4\pi}\hbar\gamma_n I_z\left(\frac{\mathbf{r}\times\mathbf{j}}{r^3}\right)_z + H_{\rm spin}, \quad (3)$$

where $\mathbf{j} = ev_F\boldsymbol{\sigma}$ is the electric current operator in graphene and $\boldsymbol{\sigma}$ is a vector of the Pauli matrices. The first term

describes the interaction of the nucleus with the orbital motion of the Dirac electrons [9], which contains I_z only as the electrons are confined in the plane. $H_{\rm spin}$ is unchanged with respect to its usual form.

The orbital term in Eq. (3) differs significantly from the usual form in Eq. (1) as the orbital magnetic moment ($\mathbf{r}\times\mathbf{j}$) replaces the usual term ($\frac{g\mu_B^*}{\hbar}\mathbf{r}\times\mathbf{p}$). This is the result of the peculiar form of the current operator for Dirac electrons $\mathbf{j}\sim\boldsymbol{\sigma}$, which is also responsible for the jittery motion of the center of mass coordinate known as *Zitterbewegung* [10]. Equation (1) can be deduced formally from Eq. (3) by using $\mathbf{j}=e\mathbf{p}/m^*$ for a normal metal.

A unique property of the orbital magnetic moment of graphene is that it remains invariant in an applied magnetic or gauge field, since $\mathbf{j}$ is insensitive to the vector potential. We mention that the proper orbital angular momentum of Dirac particles is still $\mathbf{r}\times\mathbf{p}$ in the sense that it is responsible for rotations in the x-y plane, which differs from the orbital magnetization. We also note that there are no higher order terms in the vector potential in the graphene HFI Hamiltonian due to the linearity of the Dirac equation.

The second quantized form of the orbital part of the interaction in graphene is obtained as

$$H_{\rm orb}^{\rm gr}=\frac{J_{\rm orb}}{N}I_z\sum_{\mathbf{k}\mathbf{k}'\alpha\alpha' s}f(\mathbf{k},\mathbf{k}',\alpha,\alpha')c^+_{\mathbf{k}\alpha s}c_{\mathbf{k}'\alpha' s,} \tag{4}$$

where $J_{\rm orb}=\mu_0\hbar\gamma_n e v_F/2A_c$, $f(\mathbf{k},\mathbf{k}',\alpha,\alpha')=\{\alpha\alpha'-\exp[i(\varphi_k-\varphi_{k'})]\}(\alpha k+\alpha' k')/2|\mathbf{k}-\mathbf{k}'|$, $c^+_{\mathbf{k}\alpha s}$ creates a quasiparticle with energy $E_\alpha(\mathbf{k})$ and real spin s, φ_k is the angle of $\mathbf{k}$ with the k_x axis, A_c is the unit cell area, and N is the number of unit cells. The interaction is bounded as $|f(\mathbf{k},\mathbf{k}',\alpha,\alpha')|\le 1$. The magnitude of the orbital term is estimated as $J_{\rm orb}\approx 21$ MHz using $\gamma(^{13}\mathrm{C})/2\pi=10.7$ MHz/T.

The effective HFI is obtained from Eq. (3) as

$$H_{\rm HFI}^{\rm gr}=\mathbf{S}\bar{\mathbf{A}}\mathbf{I}+H_{\rm orb}^{\rm gr}, \tag{5}$$

where $\bar{\mathbf{A}}$ is a 3×3 tensor with diagonal elements. Of these, the traceless ones are due to the spin-dipole interaction as $A_{\rm dip}(x,y){:}A_{\rm dip}(z)=-A_{\rm dip}{:}2A_{\rm dip}$, and the scalar term $A_{\rm iso}$ is given by the isotropic Fermi-contact interaction. First-principles calculations [11] gave $A_{\rm dip}=73$ MHz and $A_{\rm iso}=-44$ MHz, which gives $(-117,-117,102)$ MHz for the diagonal elements of $\bar{\mathbf{A}}$. The first-principles value of $A_{\rm dip}$ agrees well with the $A_{\rm dip}=91$ MHz obtained for the p_z orbital of a free carbon atom [12], which confirms that it is the relevant orbital.

Upon establishing the hyperfine interaction in graphene, we turn to the calculation of the NMR measurables. For a given magnetic field, terms of Eq. (5) perpendicular and parallel to the field contribute to relaxation and to the Knight shift, respectively [5,13]. The spin-lattice relaxation rate $1/T_1$ and the Knight shift K for a given magnetic field direction ($i=x,y,z$) are [14]

$$\left(\frac{1}{T_1T}\right)_i=\frac{C_i^2\pi k_B}{\hbar}\int_{-\infty}^{\infty}\frac{\rho(E^2)dE}{4k_BT\cosh^2[(E-\mu)/2k_BT]}, \tag{6a}$$

$$K_i=\frac{A_i\gamma_e}{2\gamma_n}\int_{-\infty}^{\infty}\frac{\rho(E)dE}{4k_BT\cosh^2[(E-\mu)/2k_BT]}, \tag{6b}$$

where $C_i^2=\sum_{\nu\neq i}(A_\nu^2/2+\delta_{\nu,z}2J_{\rm orb}^2)$, γ_e is the gyromagnetic ratio of electrons, $\rho(E)$ is the density of states (DOS), and μ is the chemical potential. Angular-dependent T_1 and K are obtained by standard formulas [13].

The orbital interaction involves only I_z; thus, it affects T_1 only when the field is in the graphene plane ($i=x,y$), which explains the $2J_{\rm orb}^2$ term (the 2 comes from spin degeneracy). The orbital term does not contribute to K even for a magnetic field along z in a manner analogous to demagnetization. The relaxation time for a perpendicular field due to spin-spin interaction (*without the orbital term*) would be 15% shorter than for in-plane fields. However, the orbital interaction shortens the relaxation time for an in-plane field, which results in an almost isotropic T_1. More accurate statements require the first-principles calculation [11] of $J_{\rm orb}$. The Knight shift changes sign and drops by 15% from in-plane to out-of-plane fields. We omit the i index from C_i in the following.

We discuss two scenarios for the DOS in the following: (i) absence of Landau levels and (ii) where presence of Landau levels is important. Scenario (i) occurs for three cases: when the magnetic field is in the plane, when the magnetic field is arbitrary but level broadening due to Γ or T makes the Landau levels indistinguishable around μ [the criterion is $v_F^2eB\mu\le\max(\Gamma,k_BT)$], or near the Dirac point (DP) (small μ) when the lowest Landau level is broadened due Γ or T [the criterion is $v_F\sqrt{2eB\hbar}\le\max(\Gamma,k_BT)$].

The magnetic field-free DOS is used in scenario (i):

$$\rho(E)=\frac{A_c|E|}{2\pi\hbar^2v_F^2} \tag{7}$$

per spin and C atom. The resulting relaxation rate is

$$\left(\frac{1}{T_1T}\right)=C^2\frac{\pi k_B}{\hbar}\left[\rho^2(\mu)+\rho^2\left(\frac{\pi k_BT}{\sqrt{3}}\right)\right], \tag{8}$$

which goes as $\max[\mu^2,(\pi k_BT)^2/3]$. T is important only near the DP; otherwise, μ dominates.

Exactly at the DP, T_1 diverges as $T_1\sim T^{-3}$; therefore, the nuclear spins are not relaxed by conduction electrons at $T=0$ due to the absence of charge carriers. In the presence of impurities, the DOS at the DP reads as [15]

$$\rho(0)=\frac{A_c}{2\pi\hbar^2v_F^2}\frac{2\Gamma}{\pi}\ln\left(\frac{D}{\Gamma}\right), \tag{9}$$

with Γ the scattering rate and D the cutoff in the continuum theory. Therefore, the aforementioned divergence of the clean system weakens to $T_1\sim[\Gamma^2\ln^2(D/\Gamma)T]^{-1}$, reproducing the Fermi-gas behavior.

The Knight shift is evaluated as

$$K = A\frac{\gamma_e}{2\gamma_n}\rho\left\{2k_BT\ln\left[2\cosh\left(\frac{\mu}{2k_BT}\right)\right]\right\}. \quad (10)$$

It can be approximated by $K \sim \max(2k_BT\ln 2, |\mu|)$. For undoped graphene at $T = 300$ K, this gives $|K| \approx 0.4$ ppm, which compares well with the predicted values <2 ppm on single-wall metallic nanotubes [16]. Impurities provide a finite DOS even at the DP; therefore, the Knight shift stays finite there as $K \sim \Gamma\ln(D/\Gamma)$.

Concluding scenario (i), we give $1/T_1T$ for the case of chemical doping of or chemisorption on the graphene layer. For an AC_x composition, where A is an alkali atom with full charge transfer, there is an extra $2/xA_c$ electron density to each lattice site. This translates to a chemical potential shift of $\mu = \hbar v_F\sqrt{2\pi/xA_c}$, which leads to $T_1 \approx 500\ \mathrm{s\,K} \times (x/T)$. This gives $T_1 \approx 10$ s at 300 K for $x = 8$, which is a usual doping level for graphite [17]. The Knight shift is $|K| \approx 80/\sqrt{x}$ ppm, giving $|K| \approx 28$ ppm for $x = 8$, similar to that in intercalated graphite [17] ($K = 90$ ppm for KC_8). It shows the sensitivity of the NMR properties for doping, which may lead to a sensor application of graphene. The chemical potential can be also tuned by gate voltage with a less dramatic effect on T_1.

For scenario (ii), Landau level formation is important, and the continuous spectrum is replaced by discrete Landau levels as $E_{n\alpha} = \alpha E_L\sqrt{n}$, where $\alpha = \pm$, n is a non-negative integer, $E_L = v_F\sqrt{2\hbar eB_z}$ is the Landau scale, and B_z is the perpendicular component of the magnetic field. With this, the DOS reads as [15]

$$\rho(E) = \frac{A_c}{2\pi\hbar^2v_F^2}\frac{1}{2\pi}\left[\frac{\Gamma E_L^2}{E^2+\Gamma^2} - 4\Gamma\ln\left(\frac{E_L}{D}\right) - 2\,\mathrm{Im}\left\{(E+i\Gamma)\Psi\left(1-\frac{(E-i\Gamma)^2}{E_L^2}\right)\right\}\right], \quad (11)$$

where $\Psi(x)$ is Euler's digamma function, and reduces to Eq. (7) for clean systems with a vanishing magnetic field. The $1/T_1T$ and the Knight shift are shown in Fig. 1 separately as a function of the chemical potential. These display the characteristic de Haas–van Alphen-like oscillatory behavior at high magnetic field and low μ and T that we refer to as the extreme quantum limit (EQL).

Calculation of the relaxation rate and Knight shift allows one to test the validity of the Korringa relation, i.e., whether $1/T_1TK^2 = \mathrm{const}$ holds. In general, the Korringa relation is valid for a Fermi liquid. In particular, for a noninteracting Fermi gas [18] $(1/T_1TK^2)_F = 4\pi k_B(\gamma_n/\gamma_e)^2/\hbar$. For graphene within scenario (i) and in the limit of $(\mu, k_BT) \gg \Gamma$, which is referred to as the scaling limit, it reads as

$$\frac{1}{T_1TK^2} = \frac{4\pi k_B}{\hbar}\left(\frac{\gamma_n}{\gamma_e}\right)^2\left(\frac{C^2}{A^2}\right)F\left(\frac{\mu}{k_BT}\right), \quad (12)$$

which depends only on the ratio of μ and T, and $F(x)$ is a universal scaling function

$$F(x) = \frac{3x^2+\pi^2}{12\ln^2[2\cosh(x/2)]}, \quad (13)$$

which is even in x, satisfies $F(0) = \pi^2/3\ln^2(4) \approx 1.71$ and $F(\infty) = 1$, and is shown in Fig. 2. For an in-plane field $C^2/A^2 < 1$, while for a perpendicular field $C^2/A^2 > 1$. For $\mu \gg k_BT$, the DOS is finite, and nothing distinguishes graphene from a conventional metal as only one branch of the "V"-shaped dispersion is seen at low T; therefore, the usual Korringa relation is satisfied. In the opposite limit ($\mu \ll k_BT$), the Korringa relation leads to a constant $F(0)$ times bigger than its conventional value, which signals the nature of Dirac fermions. The crossover can be explored even away from the DP by fixing the chemical potential to a finite value and sweeping the temperature. Right at the DP, impurities spoil the crossover and reestablish the Fermi-gas relation for $(k_BT, \mu) \ll \Gamma$.

The Korringa relation can be numerically evaluated in the presence of Landau levels [i.e., for scenario (ii)] using Eq. (11), and Fig. 2 shows the result. For small T and Γ, the oscillatory behavior due to Landau levels characterizes the Korringa relation. When $(k_BT, \Gamma) > E_L$, the Landau levels are smeared and the magnetic field does not play a role, and the scaling limit is restored.

In Fig. 3, we summarize the NMR properties in the form of a "phase diagram." The extreme quantum limit shows up only at low temperatures and a small chemical potential, when the Landau level structure is visible. Larger Γ, i.e., the presence of defects, favors the Fermi-gas region.

We finally comment on the feasibility of NMR experiments in graphene. NMR has a low signal sensitivity albeit its tremendous utility, and the NMR active ^{13}C nuclei has a low abundance ($c = 1.1\%$) and a low gyromagnetic ratio $\gamma(^{13}C) \approx \gamma(^1H)/4$. NMR spectrometers are characterized by the limit of detection (LOD) parameter, i.e., the number of nuclei required for a signal-to-noise ratio of three in a

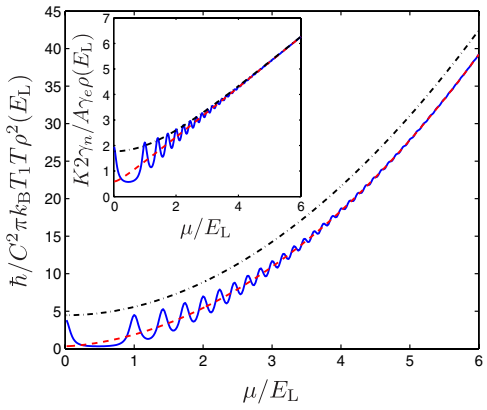

FIG. 1 (color online). The nuclear spin relaxation rate (main figure) and the Knight shift (inset) are shown with $\Gamma = 0.1E_L$ and $D = 1000E_L$ as a function of the chemical potential. The solid blue (dashed red) line refers to the presence (absence) of a magnetic field at $T = 0$, and the black dashed-dotted line corresponds to $k_BT = E_L$ in the presence of a magnetic field. Increasing μ or T makes the Landau level structure disappear.

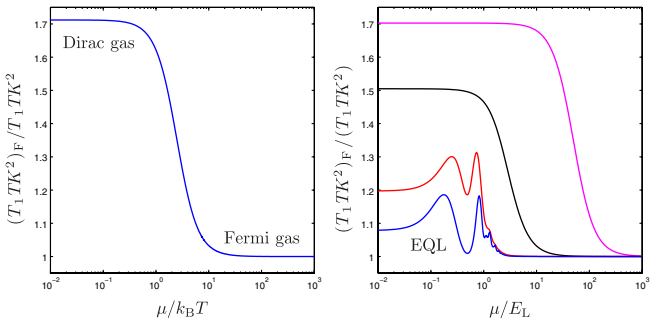

FIG. 2 (color online). The Korringa relation, normalized to its Fermi-gas value, as a function of μ/k_BT (left panel) and μ/E_L (right panel). The usual Korringa relation is recovered for $\mu \gg k_BT$, but for increasing T the normalized Korringa relation increases and saturates to $\pi^2/3\ln^2(4)$. The right panel shows the Korringa relation for $\Gamma = 0.1E_L$, which allows the visibility of the lowest Landau levels. The temperature is varied as $k_BT/E_L = 0.05$, 0.1, 1, and 20 from bottom to top. For $k_BT \sim \Gamma$, separate peaks indicate the Landau level structure, and the curves cross over to the field-free scaling limit with increasing T.

single acquisition. State-of-the-art spectrometers [20] have $\mathrm{LOD}_0 = 10^{12}/\sqrt{\mathrm{Hz}}$ for ^{1}H spins with the sample and detector at 300 K in a 14 T magnetic field [$\nu(^1\mathrm{H}) = 600$ MHz]. For a general case the LOD is [21]

$$\mathrm{LOD} = \frac{\mathrm{LOD}_0}{c}\sqrt{\frac{1\ \mathrm{sec}}{T_2^*}}\left(\frac{\gamma(^1\mathrm{H})}{\gamma}\right)^3\frac{T_s}{300\ \mathrm{K}}\mathrm{NF}_{\mathrm{rel}}. \qquad (14)$$

Here T_2^* is the decay time of the NMR time-domain signal which contains the spin-spin relaxation time T_2 and the magnetic field inhomogeneity due to defects and the magnet. The Curie T dependence of the NMR signal is described by the sample temperature T_s. $\mathrm{NF}_{\mathrm{rel}}$ is the receiver noise factor relative to a receiver at 300 K.

Clearly, low sample temperature, low detector noise, and highly ^{13}C enriched graphene are required for an NMR study. T_s of 1 K is customary in solid state NMR, and $\mathrm{NF}_{\mathrm{rel}} = 1/8$ was reported for cryo-probe NMR [22]. We estimate from NMR data on graphitic carbon [17,23] that the FWHM $= 1/\pi T_2^*$ is 50 ppm at 14 T of fully ^{13}C enriched graphene giving $T_2^* = 10$ μs. This includes a weakly anisotropic T_2 due to the nuclear spin-spin interaction, which amounts to 24 (28) ppm according to the Van Vleck formula [1], for a magnetic field perpendicular (parallel) to the graphene plane. These factors give an LOD for ^{13}C graphene of 8×10^{12} which corresponds to a surface of 0.63 mm^2. Synthesis of ^{13}C graphene with such an area (not necessarily of a single piece) is within reach as ^{13}C enriched graphite was synthesized [23]. We expect that a dedicated NMR microcoil setup prepared by lithographic methods [20] would further decrease the LOD value and the required graphene sheet area.

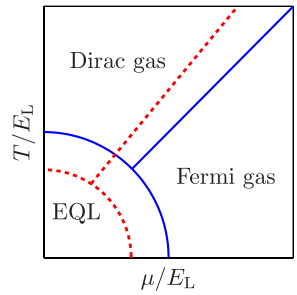

FIG. 3 (color online). Schematic phase diagram of graphene according to NMR. The boundaries (solid curves) denote smooth crossovers and move to the dashed ones for increasing disorder.

In summary, we generalized the canonical theory of hyperfine interaction between the nucleus and conduction electrons for graphene. The orbital part of the HFI differs from its usual form as it does not involve the angular momentum. We identified three distinct regimes in graphene based on the NMR measurables: Fermi- and Dirac-gas phases and the extreme quantum limit. We argue that NMR on graphene is within realistic reach.

We acknowledge discussions with P. Thalmeier, A. Ványolos, and T. Ma. This work was supported by the Hungarian Scientific Research Funds (OTKA) No. K72613 and No. F61733, by the Hungarian National Office for Research and Technology (NKTH), and by the Bolyai program of the Hungarian Academy of Sciences.

[1] C. P. Slichter, *Principles of Magnetic Resonance* (Spinger-Verlag, New York, 1989), 3rd ed.
[2] N. A. Gershenfeld and I. L. Chuang, Science **275**, 350 (1997).
[3] I. L. Chuang *et al.*, Nature (London) **393**, 143 (1998).
[4] L. C. Hebel and C. P. Slichter, Phys. Rev. **113**, 1504 (1959).
[5] A. Abragam, *Principles of Nuclear Magnetism* (Clarendon Press, Oxford, 1961).
[6] K. S. Novoselov *et al.*, Science **306**, 666 (2004).
[7] A. H. Castro Neto *et al.*, Rev. Mod. Phys. **81**, 109 (2009).
[8] P. Lee and N. Nagaosa, Phys. Rev. B **43**, 1223 (1991).
[9] J. J. van der Klink and H. P. Brom, Prog. Nucl. Magn. Reson. Spectrosc. **36**, 89 (2000).
[10] J. Cserti and Gy. Dávid, Phys. Rev. B **74**, 172305 (2006).
[11] O. V. Yazyev, Nano Lett. **8**, 1011 (2008).
[12] N. Sato *et al.*, Phys. Rev. B **58**, 12 433 (1998).
[13] J. Winter, *Magnetic Resonance in Metals* (Clarendon Press, Oxford, 1971).
[14] T. Moriya, Prog. Theor. Phys. **28**, 371 (1962).
[15] S. G. Sharapov *et al.*, Phys. Rev. B **69**, 075104 (2004).
[16] O. V. Yazyev and L. Helm, Phys. Rev. B **72**, 245416 (2005).
[17] M. S. Dresselhaus and G. Dresselhaus, Adv. Phys. **51**, 1 (2002).
[18] It is shown in Ref. [19] that neither dipolar nor orbital anisotropy affects the Korringa relation.
[19] V. P. Antropov *et al.*, Phys. Rev. B **47**, 12 373 (1993).
[20] P. J. M. van Bentum *et al.*, J. Magn. Reson. **189**, 104 (2007).
[21] C. Massin *et al.*, J. Magn. Reson. **164**, 242 (2003).
[22] P. Styles *et al.*, J. Magn. Reson. **60**, 397 (1984).
[23] W. Cai *et al.*, Science **321**, 1815 (2008).